3.7

COMPARISON OF INSTANTANEOUS TRMM SATELLITE AND GROUND VALIDATION RAIN RATE ESTIMATES

David B. Wolff[1,2]
Brad L. Fisher[1,2]
[1]NASA Goddard Space Flight Center, Greenbelt, Maryland
[2]Science Systems & Applications, Inc, Lanham, Maryland

1. INTRODUCTION

Space-borne rain rate estimates derived from data collected with two remote sensors aboard the Tropical Rainfall Measuring Mission (TRMM) satellite were compared against ground-based estimates inferred from radar data at several Ground Validation (GV) sites. The satellite rain rates were generated from the TRMM Microwave Imager (TMI), Precipitation Radar (PR) and Combined (COM) rain algorithms. The GV rain rates were obtained from the TRMM 2A53 rain maps. This study compared satellite and GV rain rates at the nominal scale of the TMI footprint. The matching criteria constrained the comparisons to the intersection of the PR orbital track with the GV radar domain, defined as within 100 km of the radar location. The matching PR, COM and GV rain rates were then averaged within a 7 km radius of each TMI footprint. The analysis was made at the same spatial and temporal scales in order to eliminate sampling biases in the comparisons and utilized data covering the period from 1999 to 2004. The results show that the respective rain rate estimates agree well, with some exceptions, which were associated with heavy rain events in which one or more of the algorithms failed to properly retrieve extreme rain intensities. Also, it is shown that there is a preferred mode in the TMI rain rate distributions over the ocean at or near 2 mm hr^{-1}, which is not evident in any of the other distributions. This mode was noted over ocean areas of Melbourne, Florida and Kwajalein, Republic of the Marshall Islands.

2. GROUND VALIDATION DATA

The TRMM GV program's main operational task is to provide quality-controlled rainfall products for four primary sites representing different climatic regimes: Darwin, Australia (DARW); Houston, Texas (HSTN); Kwajalein, Republic of the Marshall Islands (KWAJ); and, Melbourne, Florida (MELB). Geographical maps of the gauge and radar networks at DARW, HSTN, KWAJ, and MELB are provided in Fig. 1. The TRMM GV program is fully documented in Wolff et al. (2005), and includes site and product descriptions, as well as algorithms and data processing techniques. The GV rain products provide quasi-continuous long-term coverage at a higher spatio-temporal resolution than can be observed with the satellite, and subsequently provide an empirical means of directly validating the satellite rain estimates, along with other structural and dynamical features associated with propagating rain systems. The TRMM 2A-53 instantaneous rain maps used in this study are distributed to the scientific community through the Goddard Earth Sciences Data and Information Services Center (GES-DISC). The 2A-53 rain maps cover a continuous region extending 150 km from the given GV radar and are generated at a resolution of 2 km x 2 km with the radar located at the origin

Passive microwave rain retrievals are most accurate over the oceans because the homogeneous surface background emissions can be more clearly distinguished from atmospheric emissions associated with clouds and precipitation. The geographical maps shown in Fig. 1 illustrate one of the key operational dilemmas of TRMM GV: namely, that principally ocean sites, such as KWAJ, that provide the most physically robust comparisons for passive microwave (PM) retrievals instruments on TRMM, provide only limited real estate for deployment of gauges that can be used for calibration and validation of the GV radar rainfall estimates. GV sites with substantial gauge coverage, on the other hand, such as DARW, HSTN and MELB, lack extensive ocean coverage and contain significant coastal areas, over which it is inherently difficult, if not futile, for PM algorithms to robustly

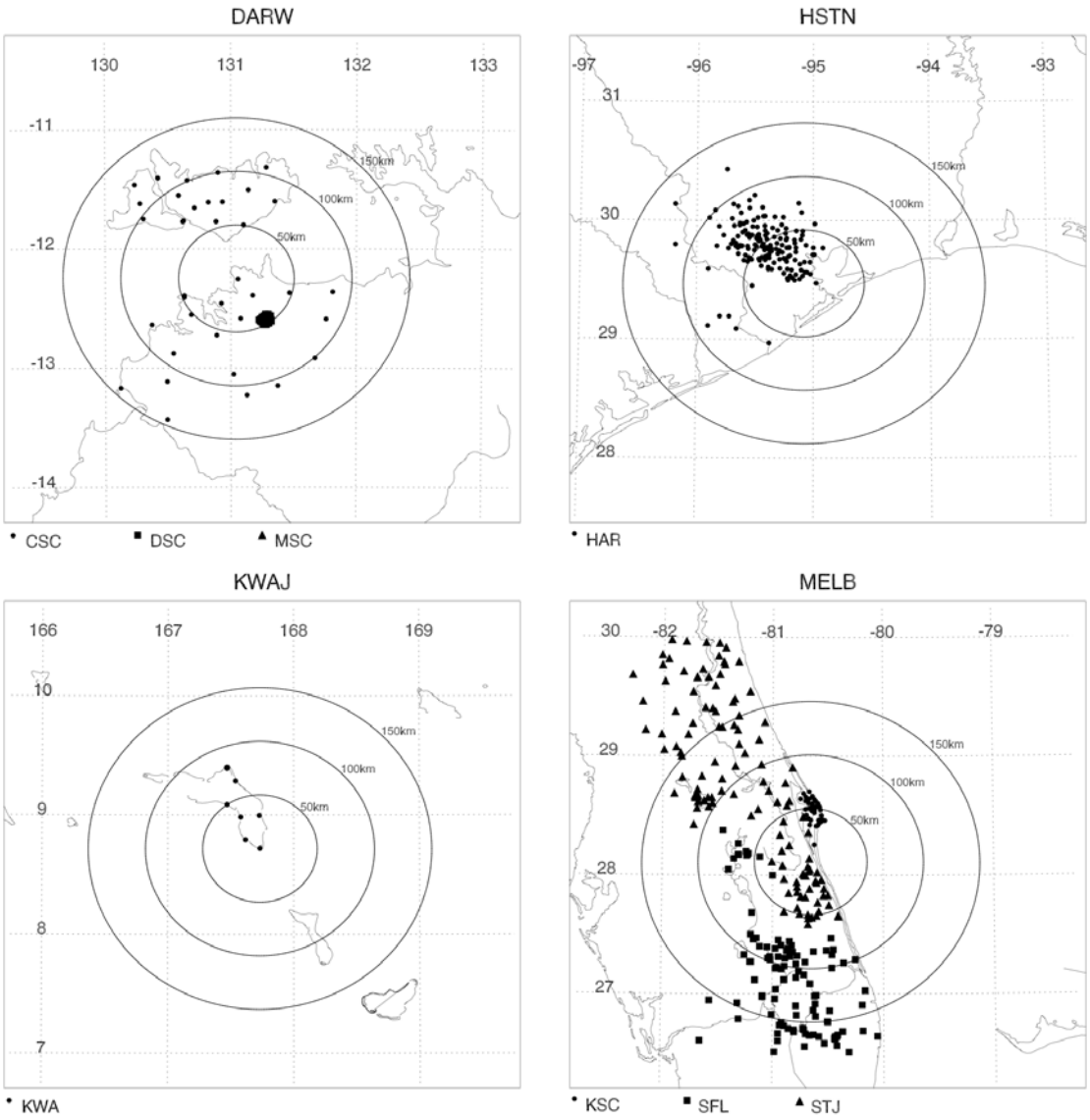

Fig. 1: Map illustrating the gauge and radar networks at GV sites: Darwin, Australia (DARW), Houston, Texas (HSTN), Kwajalein, Republic of the Marshall Islands (KWAJ) and Melbourne, Florida (MELB). Rings show distance from GV radar at increments of 50 km.

estimate rain intensities over land (over land the TMI rain estimates are inferred using only the high frequency scattering channels). Although it has been shown that there are problems with current PM physical algorithms in coastal areas (McCollum and Ferraro 2002), we will show that the full-GV-area probability distributions of rain rates are dominantly affected by coastal algorithm uncertainties, and comparison to or validation of TRMM estimates without removing estimates near coastlines can bias the results, leading to misinterpretation.

The land/coast/ocean 1/6th degree surface mask used by the Version 6 TMI algorithm to delineate geographical type are illustrated in Fig. 2.

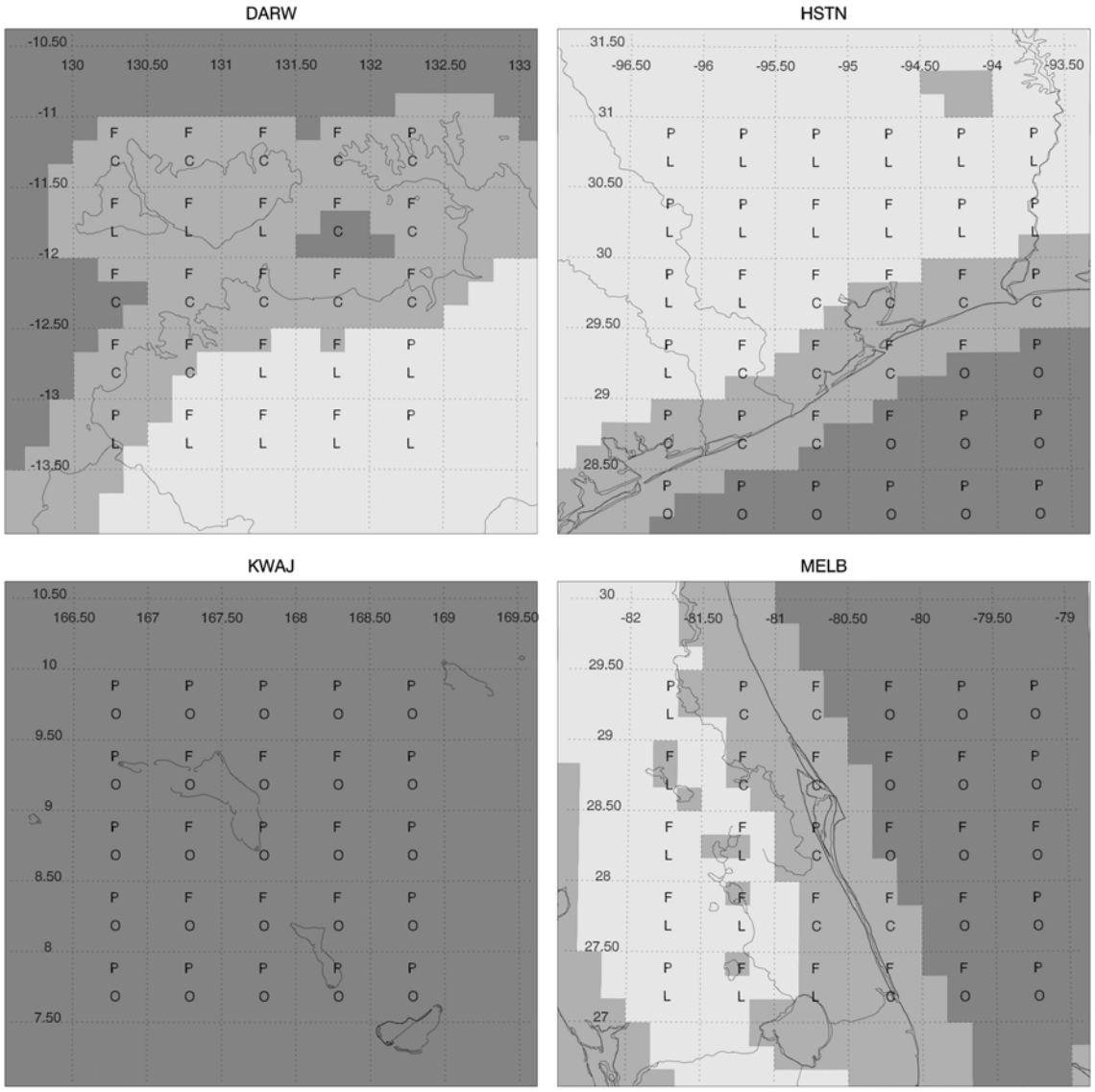

Fig. 2: Illustration of land/coast/ocean 1/6th degree mask used by the Version 6 TMI algorithm for each GV site. Shaded regions show TMI Version 6 surface mask of land (dark gray), coast (medium gray) and ocean (light gray). Also shown are the more subjectively classified 0.5° x 0.5° used for comparison of the GV data with the TRMM 3G68 product. Two character provides a GV coverage (F denotes full GV coverage, P is for partial), and geo-type of (L) land, (C) coast, and (O) for ocean.

3. TRMM SATELLITE DATA

This study used standard TRMM level II data products for the TMI (2A12), PR (2A25) and Combined (2B31) extracted over the GV validation site. Each data of these data products provides instantaneous rain rates at a geo-spatial resolution characteristic of the rain sensor. For the TMI, 2A12 product provides orbital track data that spans a swath of 759 km, with a characteristic resolution of about 154 km2, which defines the "TMI footprint." The PR and the Combined products both cover a 250 km region centered inside of the TMI track.

The Precipitation Radar (PR) is the first space-borne radar used in the collection of rain observations. The PR operates at a frequency of 13.8 GHz and has a minimum sensitivity of about 17 dBZ (~0.25 mm hr^{-1}). Its horizontal and vertical resolutions near nadir are about 4.3 km and 250 m, respectively. Its superior vertical and horizontal resolution allows the PR to observe smaller scale precipitation features that cannot be unambiguously resolved by the TMI (Kummerow

et al. 1998). However, at 13.8 GHz (2.17 cm wavelength), the PR is strongly attenuated by intervening rain.

The 2B31 product generates rain rates using the rain information contained in both the 2A12 and the 2A25 (Haddad et al. 1996)

4. SATELLITE ALGORITHMS OVER LAND, COAST AND OCEAN

The TRMM Microwave Imager (TMI) collects rain information using nine channels at five microwave frequencies: 10.7, 19.4, 21.3, 37.0 and 85.5 GHz. The 21.3 GHz is the only channel that is not dually polarized (only the vertical channel is available at 21.3 GHz). Instantaneous TMI rain rates are generated using the Goddard Profiling Algorithm (GPROF) (Kummerow et al. (2001). The algorithm has continued to evolve and significant improvements to the algorithm are described in Kummerow et al. (2001) and Olson et al. (2006).

It is important to note that distinct differences exist between the land, coastal and ocean retrievals for the various estimates. While there are inherent differences in the actual distribution of rainfall over land and ocean, much of the intra-satellite variance between the TRMM estimates over ocean and land is due to the physical assumptions and intrinsic uncertainties of the retrieval algorithms; namely, the over-ocean TMI algorithm determines surface rain rate based on theoretical physical models, while the land algorithm infers rain rate based on an empirical methodology (Spencer 1989, Wilheit et al. 2003).

The TMI algorithm relates brightness temperature to rain rate using Bayesian statistical methods. The over-ocean algorithm uses all nine available channels; the five different frequencies provide an effective vertical sounding of the cloud properties inside of the rain column. The algorithm searches a large database of cloud radiation model simulations to find cloud profiles that most closely matches the observed set of microwave radiance measurements. The physical properties of these profiles are then used to obtain a best estimate of surface rain rate (Tao, et al. 1993, Olson et al. 2006

The TMI rain algorithm over land only utilizes rain information from the two 85.5 GHz “ice-scattering” channels. The high frequency channels measure a brightness temperature depression associated with a reduction in received radiation by the satellite due to ice-scattering processes aloft. This ice scattering signal is then matched to a rainfall rate using statistically determined empirical relations between ice aloft and rainfall at the base of the cloud (Wilheit et al. 2003). Although the lower frequency channels more directly probe the precipitable water at the lower regions of the cloud, these cloud properties have to be distinguished from upwelling microwave emissions from the earth’s surface. Consequently, these channels become contaminated due to the highly varying emissions from the surface and cannot be used to determine rain rate over land (i.e., non-homogeneous background). Spencer (1989), Conner and Petty (1998) and others have shown that the high frequency scattering channels are correlated with surface rain rates and therefore can be used as an estimator of rain rate, but since the rain information is communicated by ice-scattering processes that occur above the freezing layer, the relationship between brightness temperature and rain rate is more uncertain. These brightness temperatures are also sensitive to the specific characteristics of the observed rain system.

These problems are further exacerbated over coastal areas, where ambiguity over the water/land contribution to each footprint becomes problematic from a methodological standpoint, because for either land or water. As McCollum and Ferarro (2005) note, adding the wrong surface into the footprint has the same effect on observed brightness temperature TB as rain (i.e. over land, adding surface water to the footprint will reduce TB, as does scattering by rain, and adding land to a water footprint will increase the TBs similarly to rain over water.

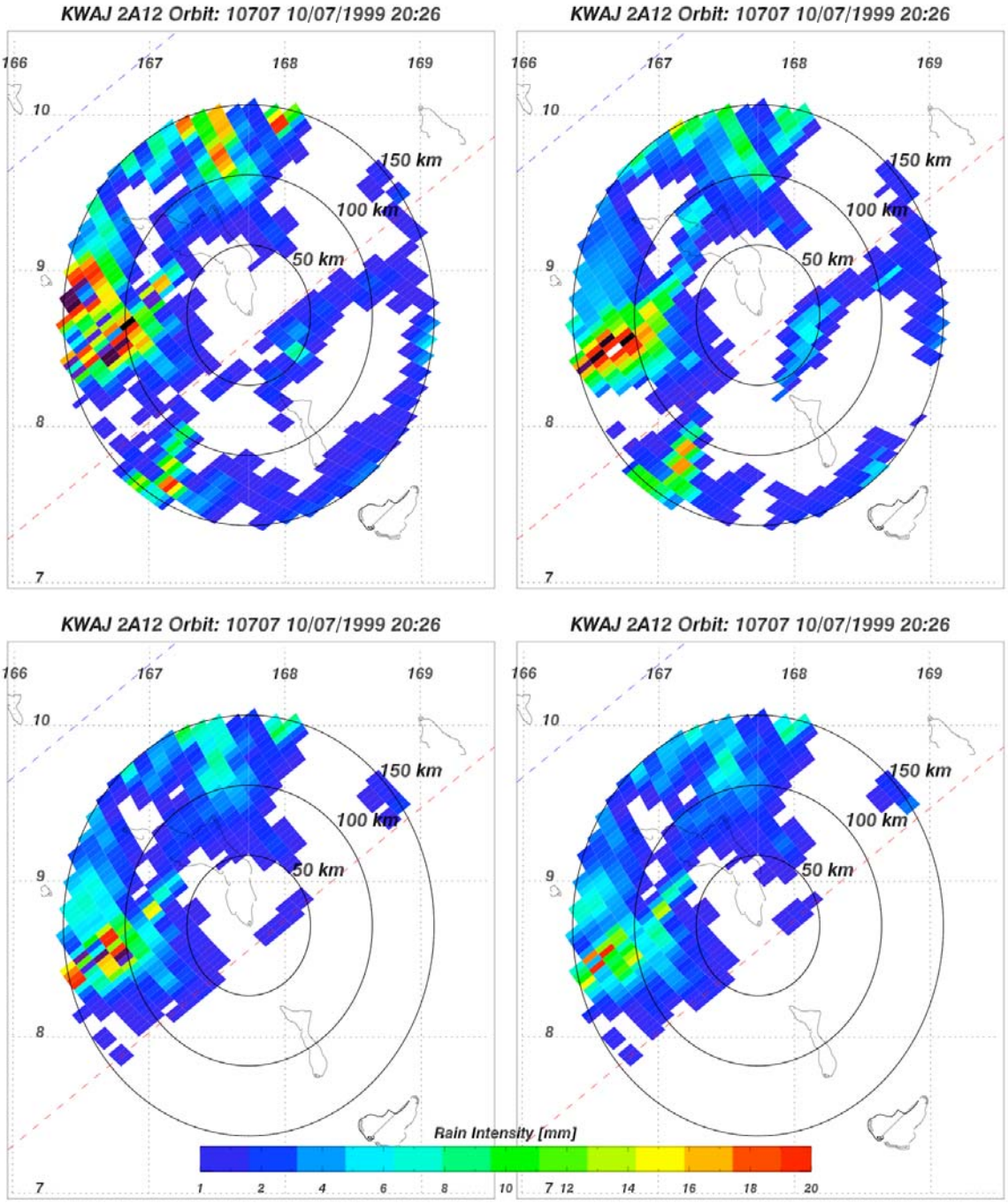

Fig. 3: Same as Fig. 9, except the GV, PR and COM data have been averaged within each TMI footprint.

The PR rain algorithm applies a path attenuation correction to the measured reflectivity using the surface reference technique (SRT) to produce an effective reflectivity factor, which is then used to estimate surface and near-surface rain rates (Iguchi et al. 2000; Meneghini et al. 2000). The SRT naturally constrains the PR field of view (FOV) to a narrow cross-track swath of 250 km (i.e., cross-track scanning angles within 17° of nadir). The attenuation correction can be a significant source of error in heavy rainfall. The spatial sampling of the PR and TMI differ due to differences in areal coverage of each sensor within the orbital track of the satellite, which leads to an expected sampling error for the PR that is about 1.3 times greater than the TMI.

The PR does not explicitly depend on the TMI geo-regional ocean, land coast classification, but differences between Z-R relations characteristic of these different regimes still need to be taken into account.

5. VALIDATION AT THE TMI FOOTPRINT SCALE

Level II TMI, PR, and COM instantaneous rain rates were matched at the scale of the TMI footprint are statistically compared to Level 2A53 GV radar rain rates at Kwajalein and Melbourne, two sites exhibiting quite different rain climatologies. The data set consisted of six years of overpasses (1999-2004). More than 50,000 pixels were available for each GV site, providing a sufficiently large sample for statistical analysis. The TMI footprint in the Level II rain products is about 154 km^2; however, TMI rain rates are determined from passive microwave radiances collected at five different frequencies, which span a broad range of geo-physical scales and collectively probe the brightness temperature structure of the atmosphere at different depths (Kummerow et al. 1998, Kummerow et. al. 2006). The Level II TMI footprint cannot therefore be thought of as representing a fundamental physical scale, but rather results from an empirical optimization of the rain information covering several different geophysical scales (Olson et al. 2006). For example, the effective field of view at 10 GHz is 67 x 37 km^2, whereas at 85 GHz the field of view is 7 x 5 km^2.

To simplify the procedure, we matched GV, PR and COM to the TMI by considering a 7 km radius around the center of the TMI footprint location. Mean rates were then computed for the GV, PR, and COM at the TMI footprint scale by locating all of the pixels (rainy and non-rainy) found within this circular region (i.e. unconditional averaging). Figure 10 illustrates the same instantaneous snapshots as Fig. 9, but after the GV, PR and COM rain rates were averaged within the respective TMI footprint areas.

The number of GV, PR and COM pixels associated with each TMI footprint vary from case to case, but tend to average about 8 for the PR and COM (native resolution of ~4.3 km x 4.3 km ≅ 18.5 km^2 resolution) and about 36 for the GV (native resolution of 2 km x 2 km = 4 km^2 resolution). The TMI surface flag was also recorded for each set of matching pixels according to whether the TMI pixel was labeled ocean, land or coast, as described previously.

5.1 Probability Distributions At The TMI Footprint Scale.

Figure 4 provides the PDF and CDF rain rates for each estimate at the footprint level at KWAJ.

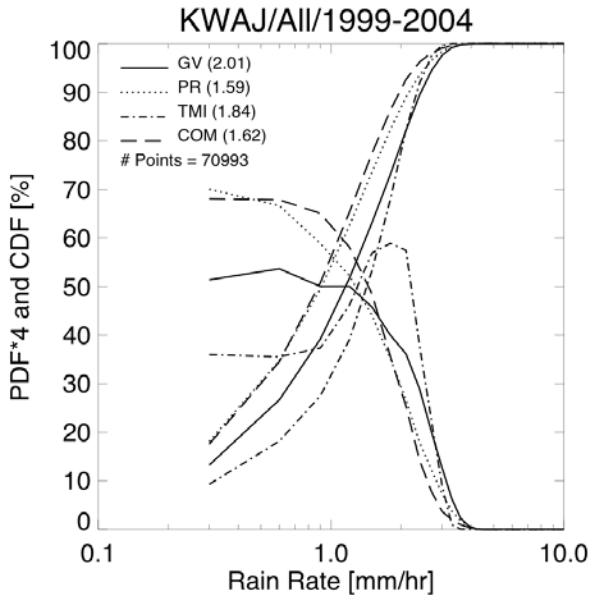

Fig. 4 PDF and CDF of rain rates for GV (solid), PR (dot), COM (dash-dot) and TMI (dash) estimates using 0.5° resolution for the period 1999-2004 at KWAJ at the TMI footprint scale.

Also, shown are the resultant mean rain rates (2.01, 1.59, 1.83 and 1.61 for GV, PR, TMI and COM, respectively), as well as the total number

of 'footprints' that were used for averaging the various estimates. Given the large number of points available for generating these distributions, much can be deemed by analysis of the individual PDFs. Most notably, note that the basic shapes of the GV, PR and COM distributions are quite similar, with rather flat unimodal peaks near 0.5 mm hr^{-1}; however, the TMI distributions is much more peaked with a pronounced mode at about 2 mm hr^{-1}.

Overall, the COM and PR CDFs agree the best, and the TMI estimates are considerably higher at all rain rates up to about the 90th percentile (just over 2 mm hr^{-1}).

Figure 5 provides the PDF and CDF rain rates for each estimate at the footprint level at MELB.

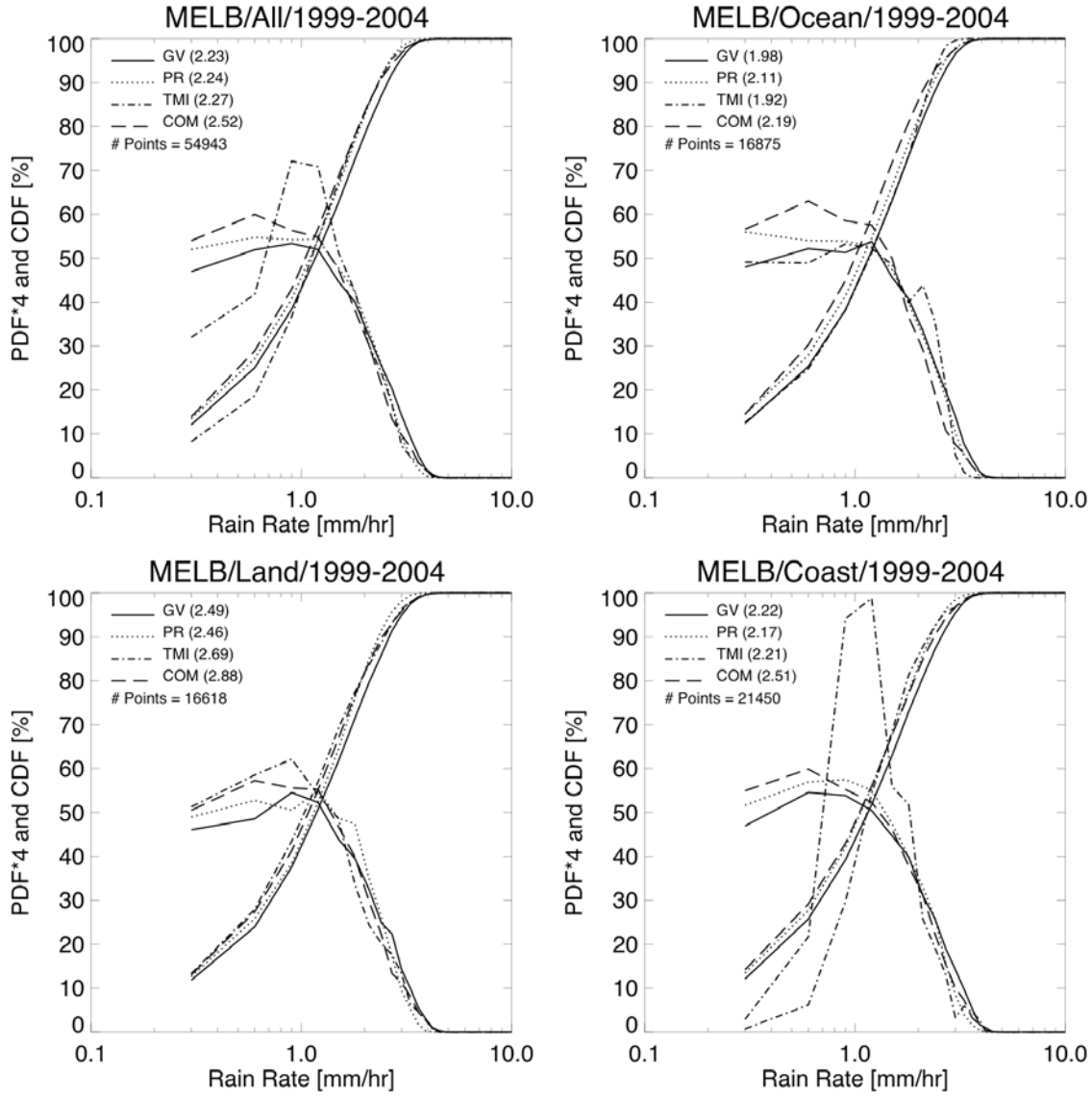

Fig. 5: PDF and CDF of rain rates at MELB at the TMI footprint scale for the period 1999-2004 showing GV (solid), PR (dot), COM (dash-dot) and TMI (dash). Top left panel shows the full GV area; top right panel is for ocean areas only; bottom left panel is for land areas only, and the bottom right is for land areas only.

The top left panel shows the overall PDF/CDF for all land types. The other panels show the PDF/CDF for Ocean, Land and Coast in the top-right, lower-left and bottom-right panels, respectively. The overall PDFs show that while the PR, COM and GV PDFs are quite similar,

the TMI PDF is significantly different In that a rather pronounced mode exists at about 1 mm hr^{-1}. This mode is even more pronounced in the Coastal PDF, illustrating the dominant effects the uncertainties in the passive microwave coastal rain estimates has on the overall PDFs, and should remind other users of the data to be wary of including coastal areas in their analyses. Over ocean and land, all of the PDFs agree fairly well, but once again a secondary mode of 2 mm hr^{-1} is evident in the TMI PDFs over ocean.

6. SUMMARY AND CONCLUSIONS

A comparison of TRMM satellite and GV rain intensity data was conducted for the period 1999-2004 at the nominal scale of the TMI footprint. It was shown that all of the estimates agree well, but there were some notable differences. Some of the discrepancies were shown to be dependent on the geographical terrain over which the various estimates were made. Over land, for example, the TMI algorithm cannot resolve light rain rates (less than approximately 0.8 mm hr^{-1}) because the algorithm only uses the 85 GHz scattering signal and this precipitation tends not to be highly correlated with ice processes aloft. The TMI coastal algorithm was also shown to have problems due to the partitioning of these regions into land and ocean sectors. This poses an intrinsic problem for GV efforts, given that most GV sites consist of a much higher fraction of coastal pixels relative to the complete sampling domain of the TRMM satellite. In the case of the PR, on the other hand, attenuation of the high frequency radar signal limits the ability of the PR to resolve areas of deep convection over land and to some extent over ocean. Over ocean, the TMI is better able to resolve the lighter rain rates (about 0.02 mm hr^{-1}), but the precipitation signal in the lower channels becomes saturated at higher rain rates (approximately 20 mm hr^{-1}).

This analysis showed that the PDFs of the GV, PR and COM were quite similar to one another; however, the TMI PDFs were significantly different. One of the key findings of this work is the pronounced effect that coastal areas have on the retrieved distribution of rain rates, especially by the TMI. Although it is well known that there remain problems to resolve with current passive microwave techniques with respect to the estimation of rain intensities over coastal areas, it was shown that the full-GV-area probability distributions of rain rates are strongly influenced by coastal algorithm uncertainties. Consequently, validating TRMM estimates without removing coastal estimates will significantly increase the quantitative uncertainty, and at the very least, lead to a misinterpretation of the results.

7. ACKNOWLEDGEMENTS

This work was funded by NASA Grant NNG07EJ50C. The authors would like to thank Dr. Ramesh Kakar (NASA Headquarters), Dr. Robert Adler (TRMM Project Scientist) and Mr. Richard Lawrence (Chief, TRMM Satellite Validation Office) for their support of this effort. We also appreciate the support staff of the TSVO, including David Makofski, Bart Kelley, David Marks, David Silberstein, and Jason Pippitt.

8. REFERENCES

Conner M.D., and G. W. Petty, 1998: Validation and intercomparison of SSM/I rain-rate retrieval methods over the continental United States. *J. Appl. Meteor*., **37**, 679-700.

Haddad, Ziad S., Eastwood Im, Stephen L. Durden, Scott Hensley, 1996: Stochastic Filtering of Rain Profiles Using Radar, Surface-Referenced Radar, or Combined RadarRadiometer Measurements. *Journal of Applied Meteorology*: Vol. 35, No. 2, pp. 229-242.

Iguchi, T., T. Kozu, R. Meneghini, J. Awaka, K. Okamoto, 2000: Rain-profiling algorithm for the TRMM precipitation radar. *J. Appl. Meteor*., **39**, 2038-2052.

Kummerow, C., 1998: Beamfilling errors in passive microwave rainfall retrievals. *J. Appl. Meteor*., **37**, 356-369.

Kummerow, C., and Coauthors, 2001: The evolution of the Goddard profiling algorithm (GPROF) for rainfall estimation from passive microwave sensors. *J. Appl. Meteor.*, **40**, 1801-1820.

McCollum, J. R., R. R. Ferraro, 2005: Microwave rainfall estimation over coasts. *J. Atmos. and Oceanic Technol.* **22**, 497–512.

Meneghini, R., T. Iguchi, T. Kozu, L. Liao, K. Okamoto, J. A. Jones, J., Kwiatkowski, 2000: Use of the surface reference technique for path attenuation estimates from the TRMM precipitation radar. *J. Appl. Meteor*., **39**, 2053-2070.

Olson, W. S., and Co-authors, 2006: Precipitation and latent heating distributions from satellite passive microwave radiometry. Part I: Improved method and uncertainty estimates. *J. Appl. Meteor*., 702-720.

Spencer, R., W. H. Goodman, and R. E. Hood, 1989: Precipitation retrieval over land and ocean with the SSM/I: identification and characteristics of the scattering signal. *J. Appl. Meteor*., **6**, 254-273.

Tao, W.-K., and J. Simpson, 1993: Goddard Cumulus Ensemble Model. Part I: Model description. *Terr. Atmos. Oceanic Sci.,* **4**, 35-72.

Wilheit, T., C. Kummerow and R. Ferraro, 2003: Rainfall algorithms for AMSR-E, *IEEE: Trans. Geoscience & Rem. Sensing*, **41**, 204-214.

Wolff, D. B., D. A. Marks, E. Amitai, D. S. Silberstein, B. L. Fisher, A. Tokay, J. Wang, and J. L. Pippitt, 2005: Ground validation for the Tropical Rainfall Measuring Mission (TRMM). *J. Atmos. Oceanic Technol*., **22**, 365-380.